

Octavinylsilsesquioxane-based luminescent nanoporous inorganic-organic hybrid polymers constructed by Heck coupling reaction

Libo Sun, Zhiqiang Liang,* Jihong Yu*

State Key Laboratory of Inorganic Synthesis & Preparative Chemistry, Jilin

University, Changchun, 130012, P. R. China

Email: liangzq@jlu.edu.cn; jihong@jlu.edu.cn

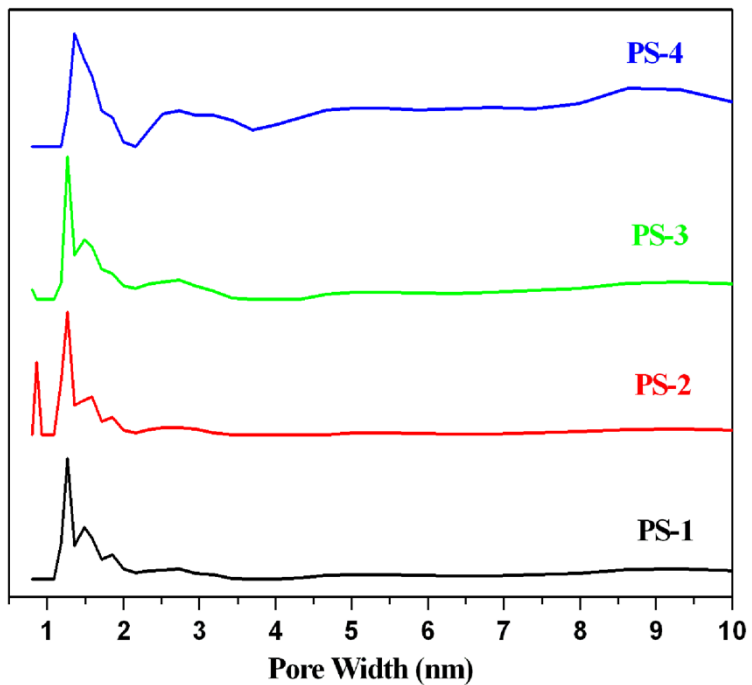


Fig. S1 The pore size distribution of **PS-n** (1-4) calculated by the NLDFT method.

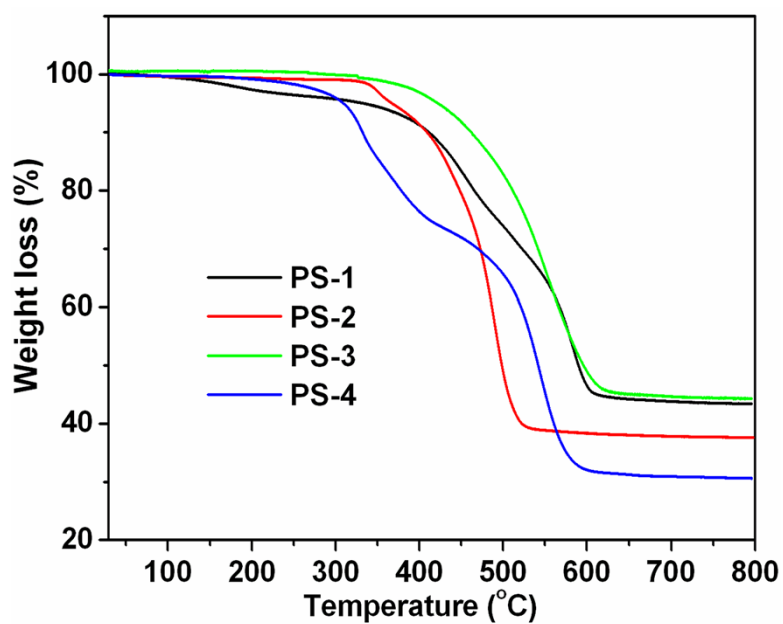


Fig. S2 TG curves for **PS-n** (1-4) under air atmosphere.

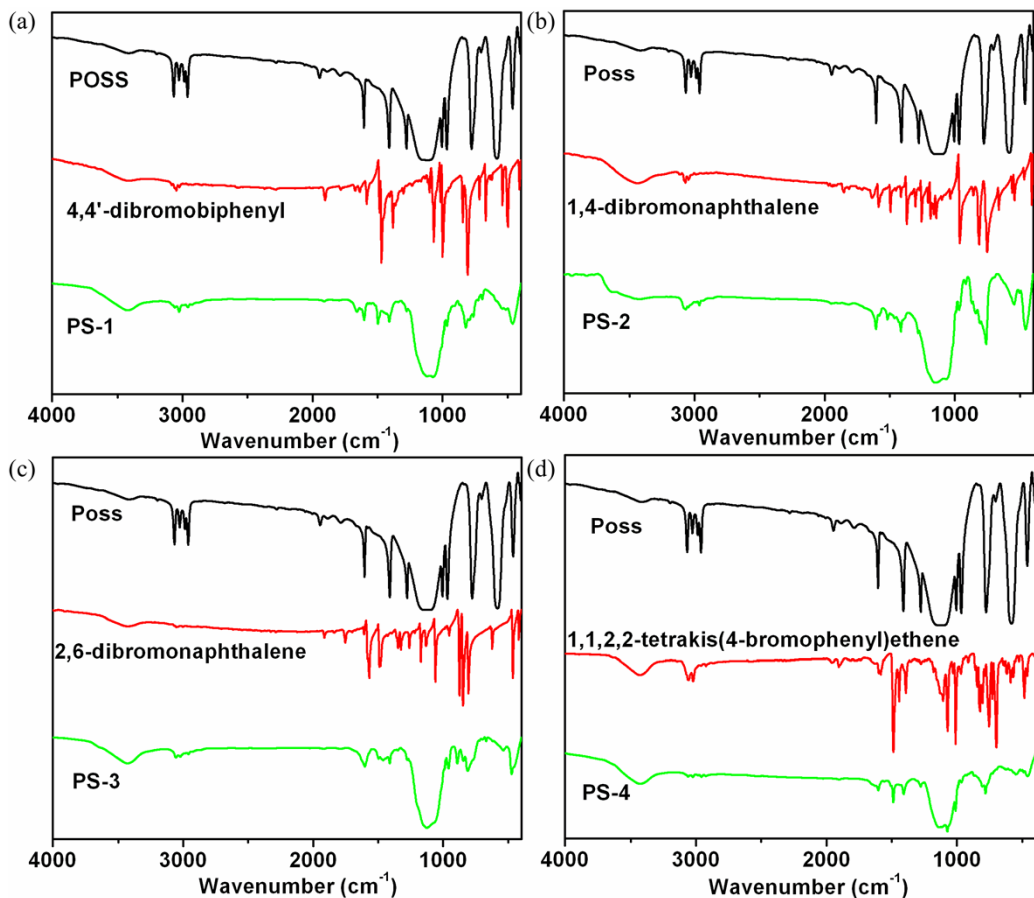


Fig. S3 FT-IR spectra of the monomers and **PS-n**: (a) monomers and **PS-1**; (b) monomers and **PS-2**; (c) monomers and **PS-3**; (d) monomers and **PS-4**.

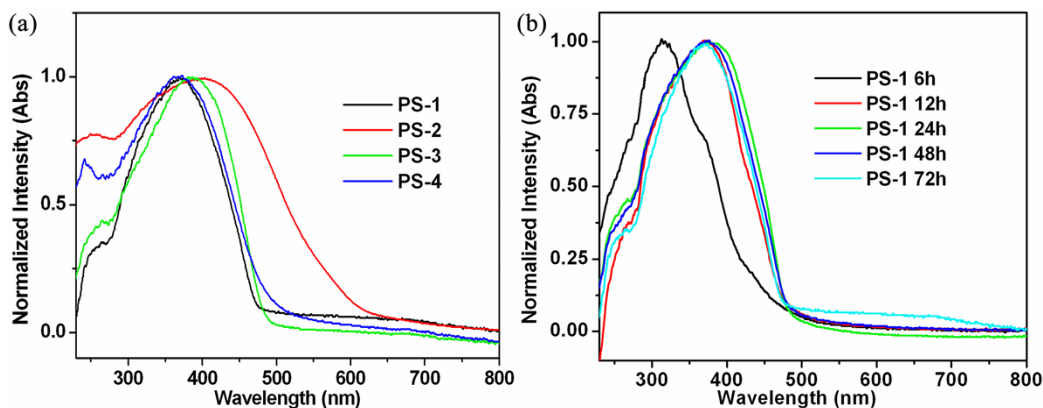


Fig. S4 (a) Solid state UV-vis absorption spectra for **PS-n** (1–4); (b) Solid state UV-vis absorption spectra for **PS-1-n** ($n = 6, 12, 24, 48, 72$ h).

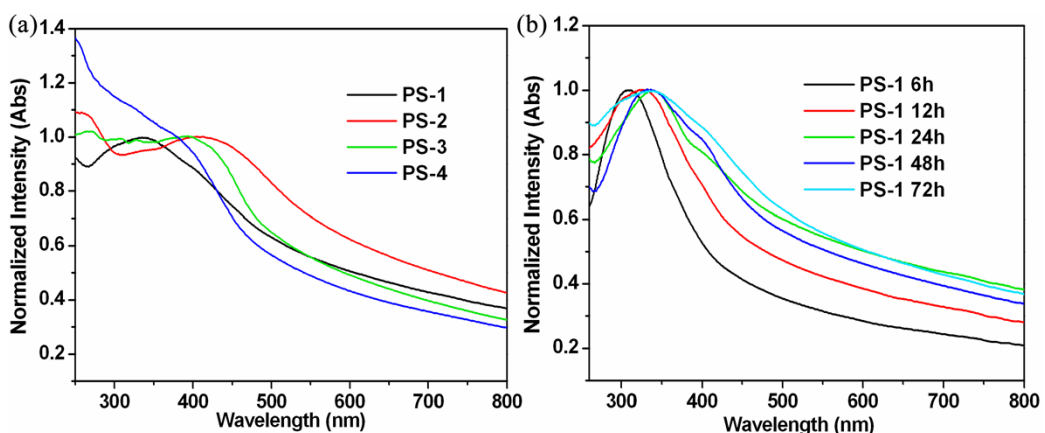


Fig. S5 (a) UV-vis absorption spectra for **PS-n** (1–4) in ethanol; (b) Solid state UV-vis absorption spectra for **PS-1-n** (n = 6, 12, 24, 48, 72 h) in ethanol.

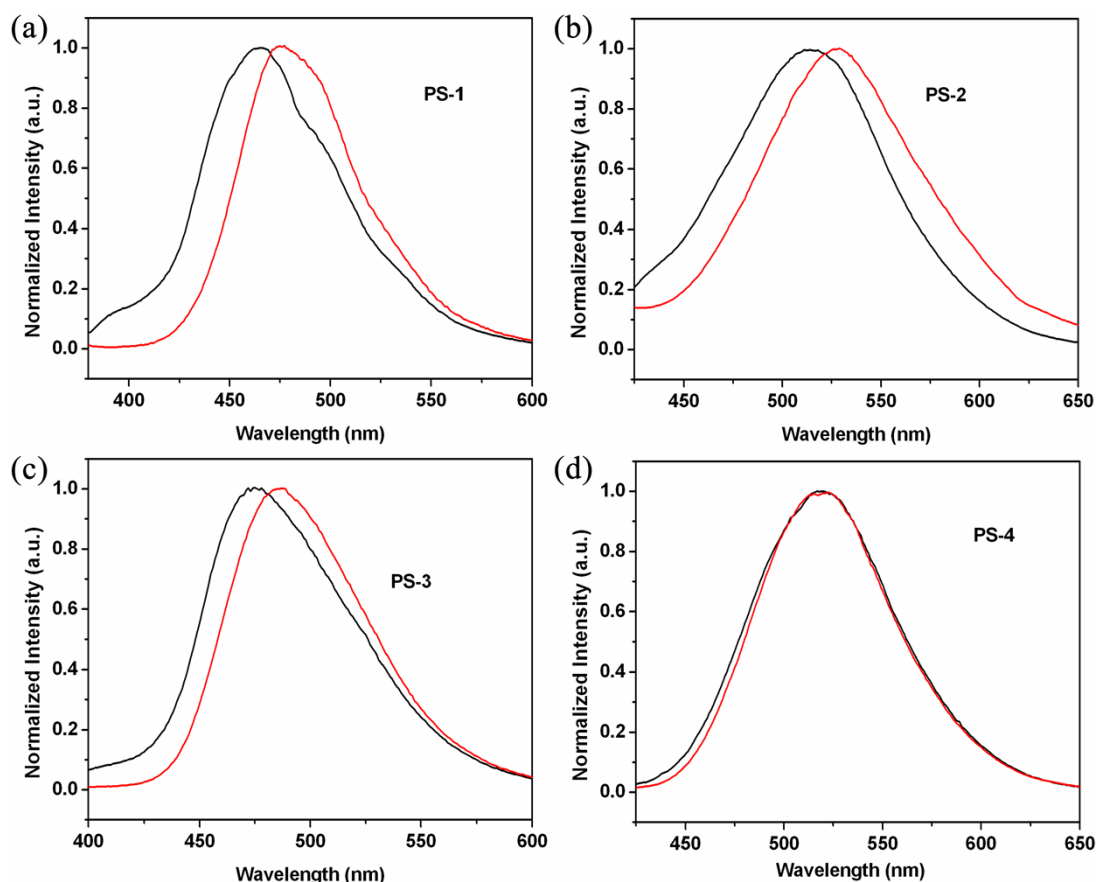


Fig. S6 Luminescent spectra of **PS-n** (1–4) in the solid state (red) and ethanol (black).

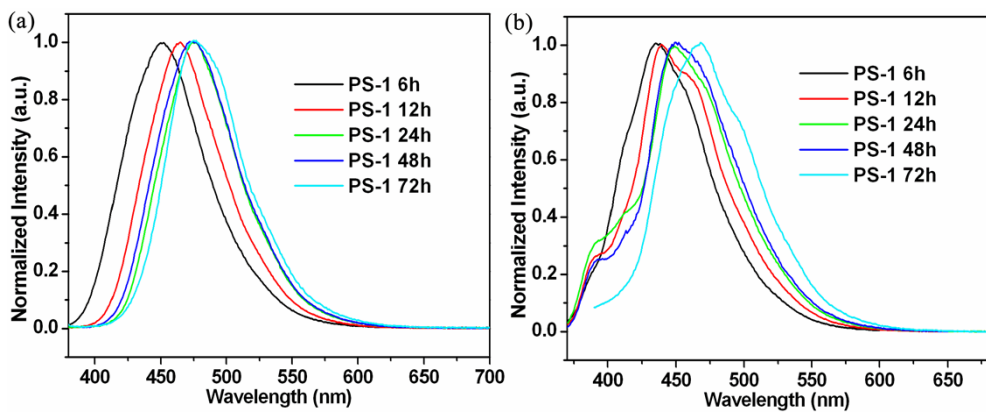


Fig. S7 Luminescent spectra of **PS-1-n** ($n = 6, 12, 24, 48, 72$ h) in the solid state (left) and ethanol (right).

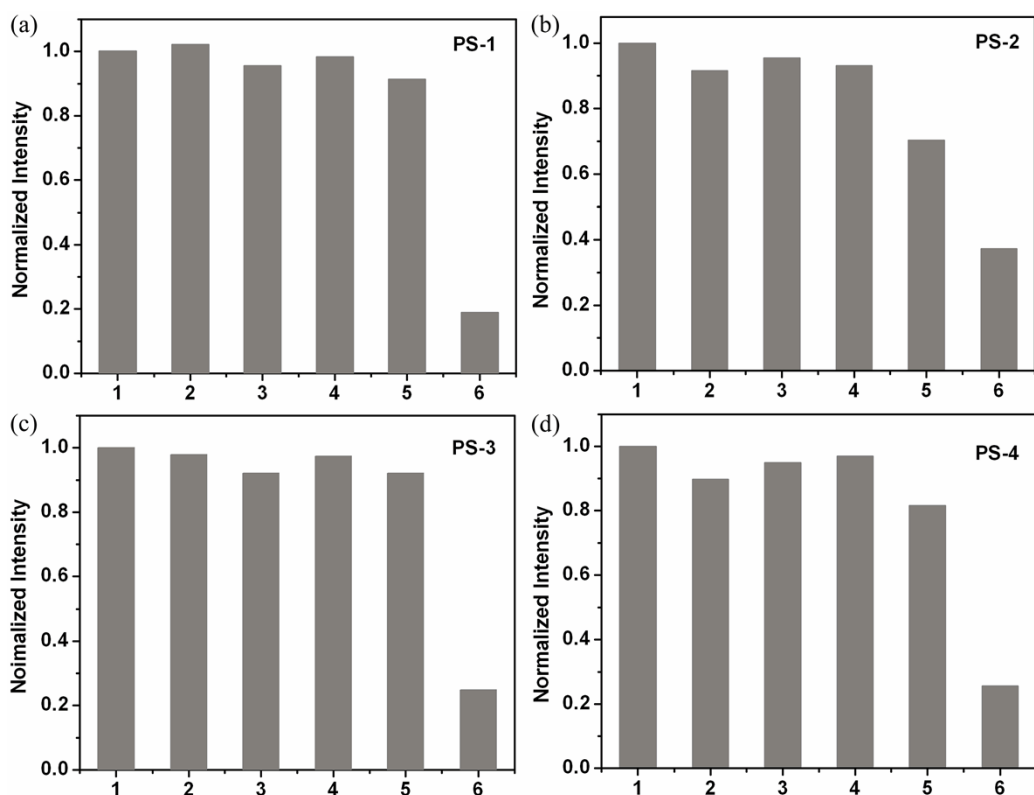


Fig. S8 The normalized luminescent intensity of **PS-n** (a: **PS-1**, b: **PS-2**, c: **PS-3**, d: **PS-4**) in ethanol (0.05 mg/mL) upon addition of ca. 46.5 μ M different analytes (1: original, 2: 2,4-dinitrochlorobenzene, 3: 2,4-dinitrotoluene, 4: 4-nitrotoluene, 5: 4-nitrophenol, 6: picric acid).

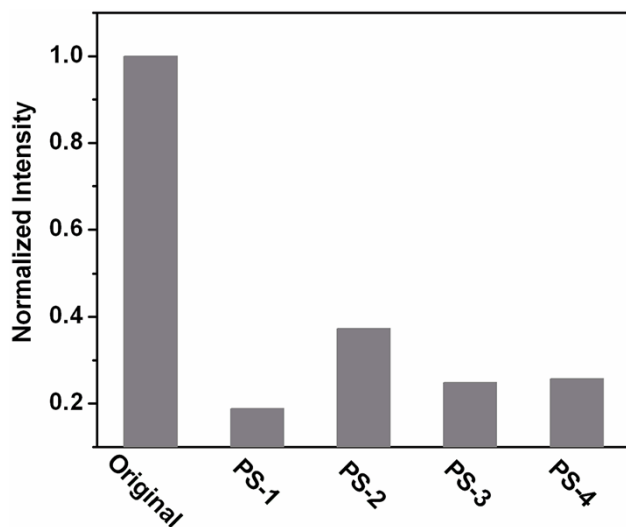


Fig. S9 The normalized luminescent intensity of **PS-n** (1–4) in ethanol (0.05 mg/mL) upon addition of ca. 46.5 μM PA.

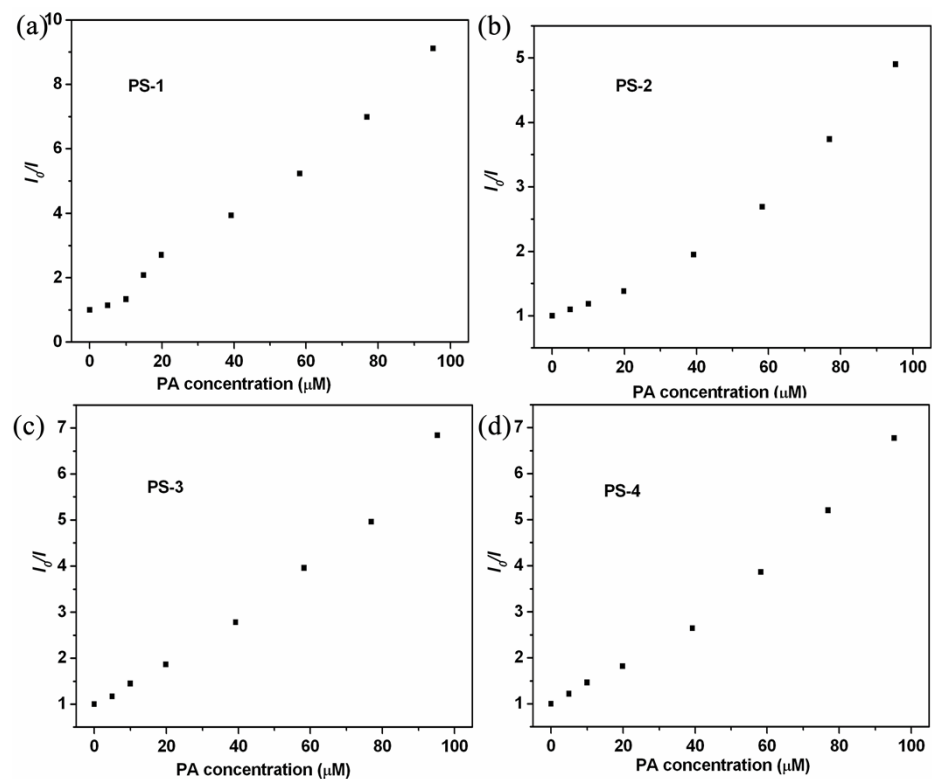


Fig. S10 The relative Stern-Volmer plots of relative PL intensity (I_0/I) versus TNP.

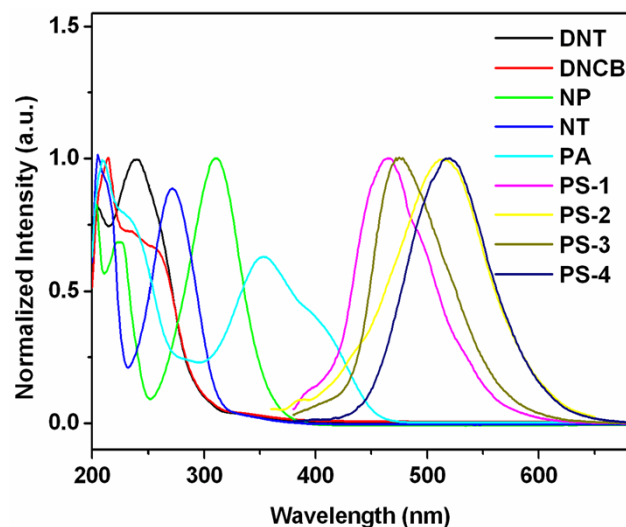


Fig. S11 Spectral overlap between the absorption spectra of analytes and the emission spectra of PS-n in ethanol.

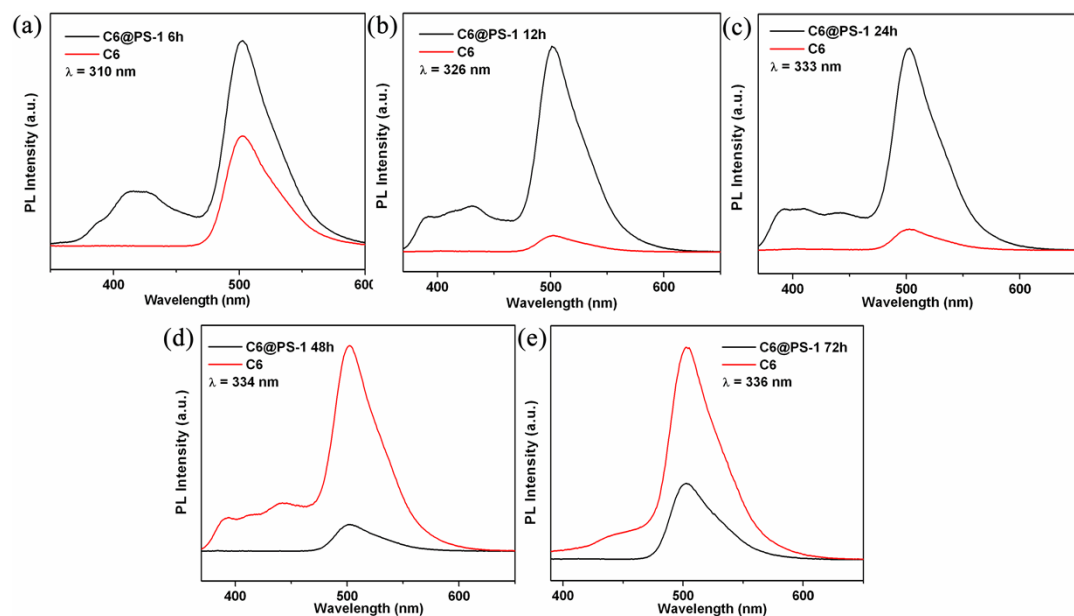


Fig. S12 Comparison emissions of C6 with and without the addition of **PS-1-n** in ethanol solution.

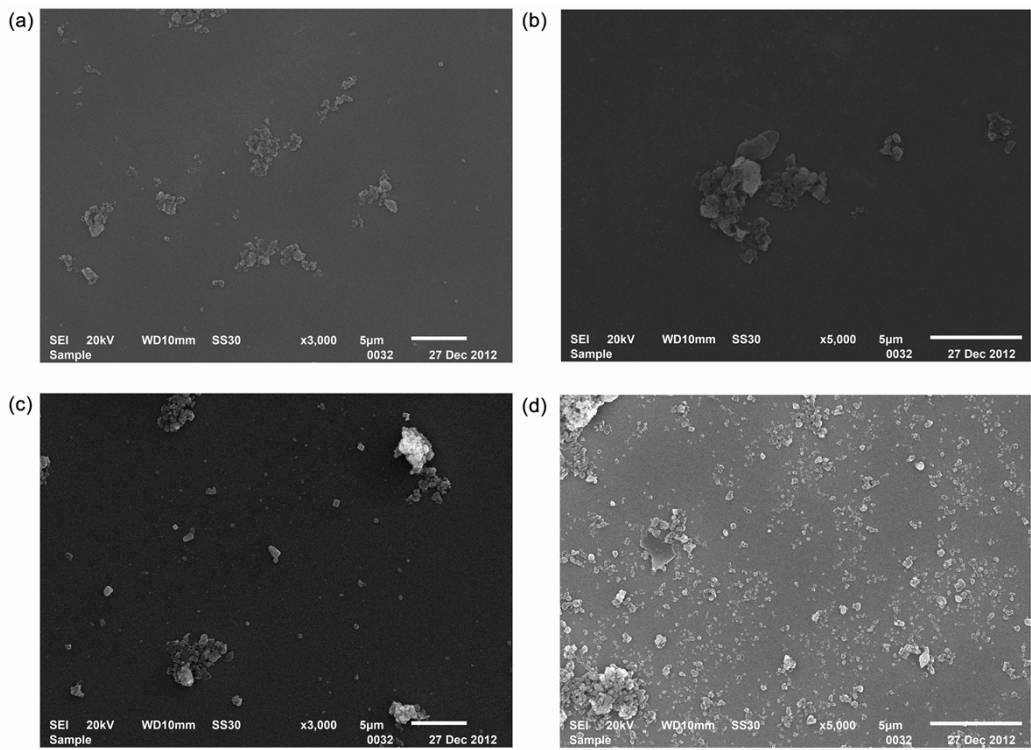


Fig. S13 Scanning electron microscope images for **PS-1** (a), **PS-2** (b), **PS-3** (c) and **PS-4** (d) at different magnifications. The samples were sputter-coated with gold before analysis.

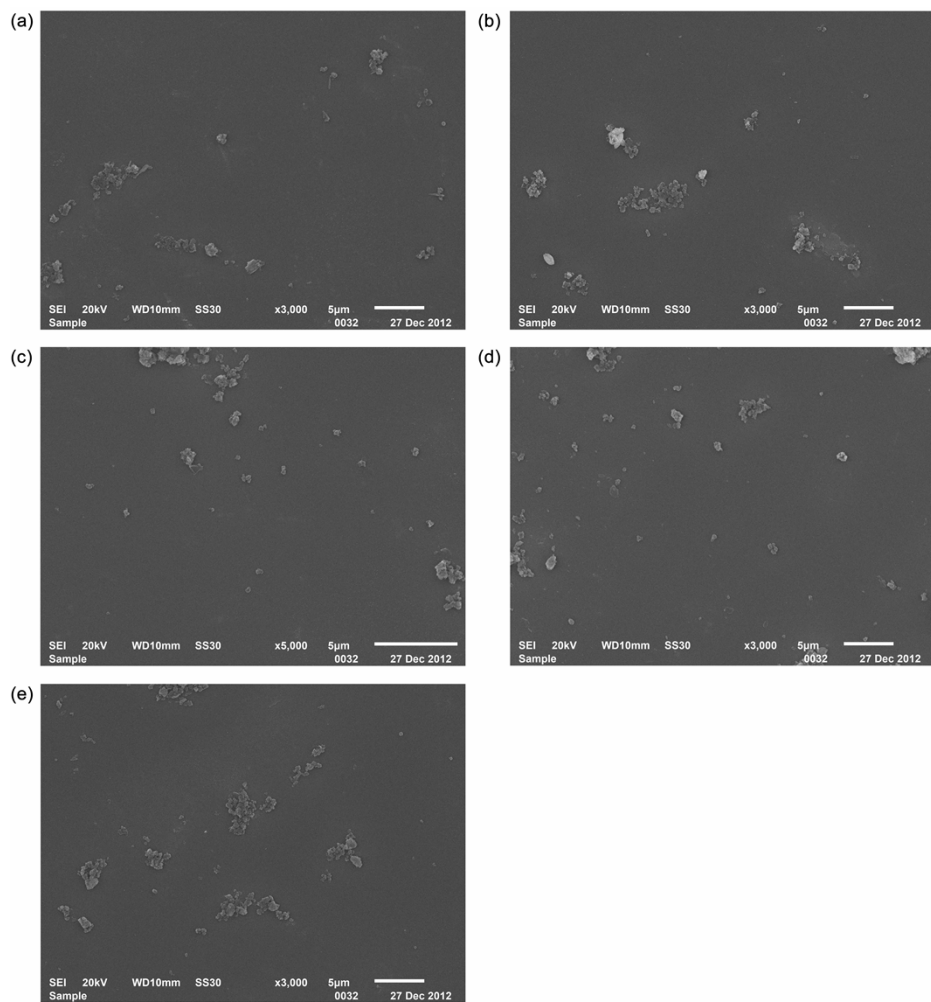


Fig. S14 Scanning electron microscope images for **PS-1** (6 h) (a), **PS-1** (12 h) (b), **PS-1** (24 h) (c), **PS-1** (48 h) (d) and **PS-1** (72 h) (e) at different magnifications. The samples were sputter-coated with gold before analysis.

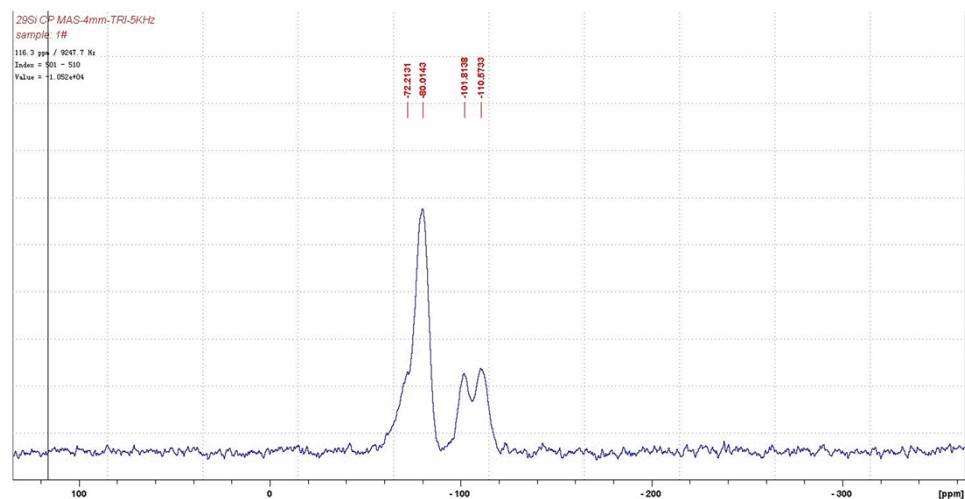


Fig. S15 The ^{29}Si NMR of **PS-1**.

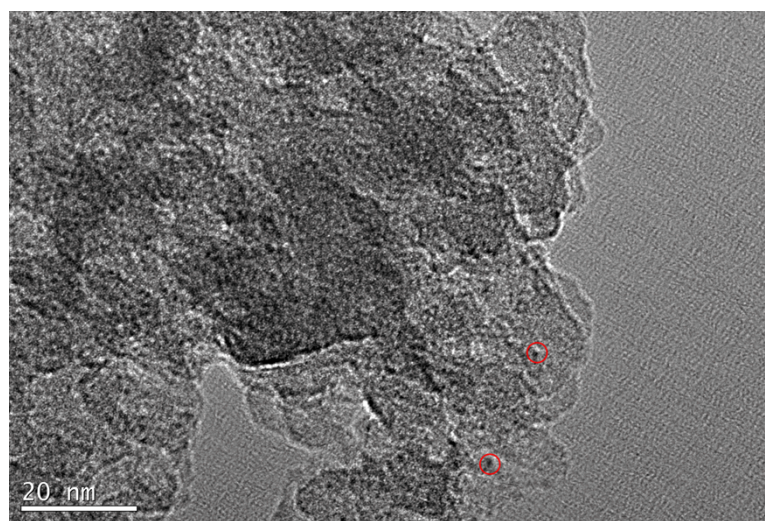


Fig. S16 The TEM image of **PS-1**. The red round cycles show the SiO_2 particles.

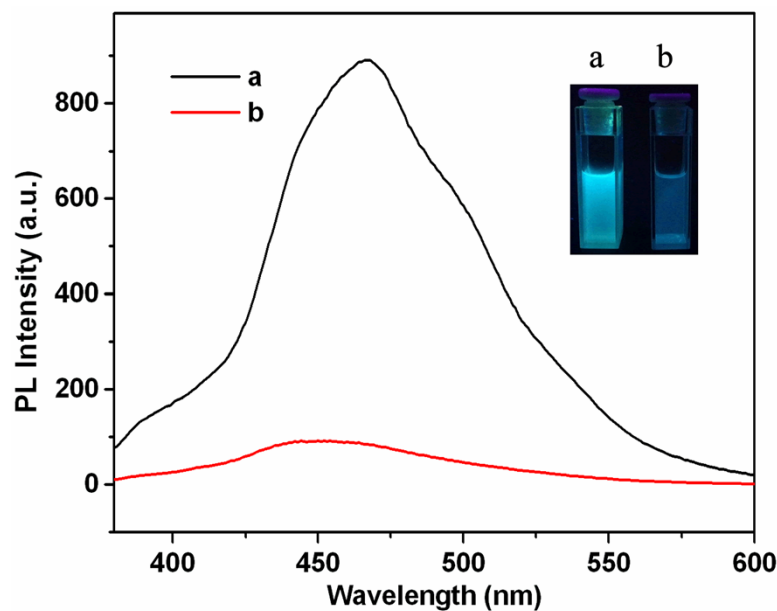


Fig. S17 Comparison emissions of **PS-1** (in ethanol solution) synthesized using our condition (a) and Feng's condition (b).

Table S1 EDX analyses of **PS-n** (1-4).

| PS-n | wt. % | | | | at. % | | | |
|-------------|-------|-------|-------|------|-------|------|------|------|
| | C | Si | Br | Pd | C | Si | Br | Pd |
| PS-1 | 40.65 | 11.11 | 0.19 | 0.48 | 66.54 | 6.21 | 0.10 | 0.05 |
| PS-2 | 44.20 | 5.22 | 13.68 | 0.14 | 71.58 | 3.62 | 3.33 | 0.03 |
| PS-3 | 46.03 | 10.58 | 1.72 | 0.45 | 65.44 | 6.43 | 0.37 | 0.07 |
| PS-4 | 39.65 | 14.28 | 3.8 | 0.18 | 62.78 | 9.67 | 0.90 | 0.06 |

Table S2 Porous properties of **PS-n** (1-4).

| PS-n | $S_{\text{BET}}/\text{m}^2 \text{ g}^{-1}$ | $S_{\text{Langmuir}}/\text{m}^2 \text{ g}^{-1}$ | $S_{\text{micro}}/\text{m}^2 \text{ g}^{-1}$ | $V_{\text{total}}^a/\text{cm}^3 \text{ g}^{-1}$ | $V_{\text{micro}}^b/\text{cm}^3 \text{ g}^{-1}$ |
|-------------|--|---|--|---|---|
| PS-1 | 550.61 | 752.32 | 212.28 | 0.543 | 0.093 |
| PS-2 | 372.79 | 502.98 | 185.23 | 0.319 | 0.084 |
| PS-3 | 685.63 | 938.08 | 182.85 | 0.760 | 0.077 |
| PS-4 | 393.95 | 544.34 | 57.85 | 0.608 | 0.021 |

^a Total volume at $P/P_0 = 0.97$.

^b The micropore volume calculated from *t*-plot method.